



Analysis of Combined Natural Convection and Radiation Heat Transfer in a Partitioned Rectangular Enclosure with Semitransparent Walls

Liqun Zhou¹ · Jiaying Liu² · Qunwu Huang¹ · Yiping Wang¹

Received: 20 February 2019 / Revised: 25 April 2019 / Accepted: 28 April 2019 / Published online: 20 June 2019
© The Author(s) 2019

Abstract

In this paper, we present a two-dimensional numerical analysis of the conjugate natural convection and radiation heat transfer in a double-space enclosure with two semitransparent walls. Two kinds of boundary conditions are considered, the first being the isothermal process of the opaque wall, and the other the incidence of a constant radiation flux in the left semitransparent wall. The renormalization group $k-\epsilon$ model is adopted to simulate the turbulent flow in the enclosure. To compute the radiation heat transfer in a semitransparent medium, the discrete ordinates model is used. We compare the behaviors of enclosures with single and double semitransparent walls and determine the difference in the results obtained for semitransparent and opaque partitions. The results indicate that a semitransparent partition facilitates a reduction in the heat loss or obtains a higher temperature distribution. The transmittance of a semitransparent wall has a great effect on the thermal and flow characteristics in an enclosure. The change of wall temperature is found to be significant when the thermal conductivity values range from 0.05 to 0.5 W/(m·K), and to be small when ranging from 0.5 to 10 W/(m·K). These conclusions are helpful for green design and energy saving in solar buildings.

Keywords Natural convection · Enclosure · Semitransparent wall · Thermal conductivity · Transmittance

List of Symbols

q	Heat flux (W/m ²)
$T_{\text{semi-left}}$	Mean temperature of left semitransparent wall (K)
$T_{\text{semi-mid}}$	Mean temperature of middle semitransparent wall (K)
c_p	Specific heat of fluid [J/(kg·K)]
g	Gravitational acceleration (m/s ²)
h	Heat transfer coefficient [W/(m ² ·K)]
I	Radiation intensity (W/m ²)

Greek Letters

λ	Thermal conductivity [W/(m·K)]
α	Thermal diffusivity (m ² /s)
β	Thermal expansion coefficient of air (1/K)

ρ	Density (kg/m ³)
ϵ_{semi}	Emissivity of semitransparent wall

Introduction

Due to its prime importance in various industrial and natural processes, determining the natural convection with radiation inside a square cavity filled with different fluids is a classical scientific problem. The model most often used to study this problem is a rectangular enclosure with two vertical isothermal walls and two horizontal adiabatic walls [1]. However, in terms of engineering applications, such as solar chimneys, double-skin facades, solar collectors, and Trombe walls, this simplified model cannot be correctly developed to investigate the flow and heat transfer characteristics [2], because the introduction of a semitransparent medium changes the enclosure characteristics. Compared to opaque materials, semitransparent materials allow a greater transmission of direct radiation. To use and understand the natural convection in buildings and systems, it is important to study the effect of a semitransparent medium on enclosures to provide references for practical applications.

Several theoretical and experimental studies have been conducted on enclosures with semitransparent walls.

✉ Qunwu Huang
huangqw@tju.edu.cn

✉ Yiping Wang
wyp56@tju.edu.cn

¹ School of Chemical Engineering and Technology, Tianjin University, Tianjin 300350, China

² Shanghai Urban Construction Material Co. Ltd, Shanghai 200063, China

Moreno and Hernández [3] presented analytical solutions for a very simple room with glazing subjected to solar radiation, in which they identified the main physical mechanisms and the importance of the indoor temperature on the spectral and thermal parameters. Flores et al. [4] presented a study of the combined heat transfer in a cubic cavity containing a vertical semitransparent wall. From this parametric study, for a fixed absorbance of a solar-control coating, the contribution of the radiative heat transfer was found to be higher than that by convection, but both the convective and radiative heat transfers were determined to increase with an increase in the ambient temperature. Li et al. [5] investigated the effect of optical constants on the conjugate laminar natural convection and radiative heat transfer in a rectangular enclosure with one vertical semitransparent wall. It was found a marked effect of the optical constants of a semitransparent wall on the laminar natural convection in a rectangular enclosure. Wu and Lei [6] developed a transient heat balance model for predicting the thermal performance of a semitransparent water-wall system. A series of studies were conducted by Xamán et al. [7–15] regarding the heat transfer in a square cavity with a semitransparent wall. By performing numerical studies of the conjugate heat transfer in a square cavity with a semitransparent wall for laminar and turbulent flows, the authors obtained a set of correlations for the Nusselt number for both laminar and turbulent flows [7, 8]. The unsteady Reynolds-averaged Navier–Stokes (URANS) model together with a low-Reynolds-number turbulence $k-\omega$ model was solved using the finite-volume method [9]. Using the glazing material available in the Mexican market, researchers have also investigated the thermal performance of a room with a double-glazed window [10, 11]. A thermal evaluation of a room with a double-glazed window both with/without a solar-control film made in Mexico was also presented [12–14]. Based on the results, we know that a room with a double-pane window with a solar-control coating is associated with a smaller heat flux than one with a window without a solar-control coating. The effect of the roofing material on a room with a semitransparent wall has also been analyzed [15].

Natural convection in a differentially heated, partitioned enclosure with an opaque partition wall occurs in various situations both in natural settings and in engineering applications. Recently, several works have outlined the heat transfer characteristics when using partitioned enclosures. Rabhi et al. [16] studied the effects of surface radiation and the number of partitions on the heat transfer and flow structures in an inclined rectangular enclosure, and found that the total heat transfer in the enclosure increased in the presence of a thermal radiation heat flux, and reduced significantly with an increasing number of partitions. Selimefendigil and Öztop [17] used the finite element method to investigate conjugate natural convection and conduction heat transfer

in an inclined partitioned cavity filled with different nanofluids on different sides of the partition. Sun et al. [18] presented extensive numerical studies on fluid flow and heat transfer in inclined and fully divided CO₂ enclosures with partitions on Mars. It was observed that three flow regimes formed in succession when the tilt angle increased, namely, Rayleigh–Bénard convection, transition convection, and single-cell convection. Sambou et al. [19] developed a one-dimensional analytical model of the coupled heat transfer (conduction, convection, radiation) in enclosures divided by multiple vertical diffusive partitions, and found that the thermal resistance could be improved by decreasing the thermal conductivity of the walls, decreasing the emissivity of the partitions faces, or using very thin partitions. Oztop et al. [20] performed numerical simulations of the conduction-combined forced and natural convection heat transfer and fluid flow in a 2D lid-driven square enclosure divided by a partition with a finite thickness and finite conductivity. It was observed there to be higher heat transfer for a higher Richardson number in an upward moving wall for all thermal conductivity ratios. Khatamifar et al. [21] studied the effects of partition thickness and position over a wide range of Rayleigh numbers, and found that the average Nusselt number increases with the Rayleigh number, but decreases with partition thickness. They also found that the partition position had a negligible effect on the average Nusselt number. Most previous studies of natural convection in partitioned enclosures have been concerned with cases where the partition wall is opaque. There is insufficient knowledge regarding enclosures with a semitransparent wall partition, as this may be a better model for many real situations.

There are also two significant points that must be emphasized in the study of rectangular enclosures. First, for most flows, the Rayleigh number often exceeds the critical values and the fluid flow becomes turbulent in many studies. However, many studies consider only laminar flows. Second, the contribution of thermal radiation is an important topic with respect to the heat transfer in enclosures. Radiation heat transfer depends on several parameters, such as the wall temperature, surface emissivity, and thermophysical properties of the internal medium. In studies of turbulent natural convection, the radiative mode of heat transfer is occasionally neglected because of the overwhelming number of computational resources it demands. However, the radiation heat transfer has a significant effect on the system and cannot be ignored, because this phenomenon occurs in numerous engineering applications. Recently, a few studies have addressed the combination of natural convection and radiation heat transfer in rectangular enclosures. Miroshnichenko et al. [22–25] conducted a series of studies on transient turbulent natural convection combined with surface thermal radiation in a square cavity with a local heater. The Rayleigh number, thermal conductivity ratio, and internal surface emissivity

have a significant effect on the temperature and stream function contours within the enclosure [22]. In addition, they found that the presence of surface radiation leads to both an increase in the average total Nusselt number and intensive cooling of this type of system. A significant intensification of convective flow was also observed by an increase in the Rayleigh number [23, 24]. The results show that an increase in the cavity inclination angle leads to a reduction in the radiative Nusselt number [25]. Turbulent natural convection in air-filled differentially heated cavities was numerically investigated using various RANS turbulence models and the discrete ordinates (DO) model [26]. The result of this study shows that the shear stress transport $k-\omega$ model performs best overall and the standard $k-\epsilon$ model has the worst overall performance. Sharma et al. [27] conducted a numerical investigation of turbulent natural convection in a transparent fluid medium and its interaction with surface thermal radiation in an inclined differentially heated enclosure. Mao and Zhang [28] conducted a numerical simulation of the turbulent natural convection of compressible air in a tall cavity, and found that the $k-\epsilon$ model had high accuracy in predicting the velocity distribution, whereas the large eddy simulation model had good performance in predicting temperature distributions.

In this study, our main aim was to investigate the effect of semitransparent walls on the natural convection flow field and temperature distribution in a double-spaced rectangular enclosure. Computation fluid dynamics can be used to simulate this problem. To compute the radiation heat transfer in a semitransparent medium, the DO model is used. The comparison of the enclosures with single and double semitransparent walls is conducted, and the difference of semitransparent partition as well as opaque partition is analyzed. The impact of different transmittance combinations on the semitransparent wall is examined. In addition, the influence of different thermal conductivities in a semitransparent medium on the performance of the proposed enclosure is also detailed.

Model Description

The study is focused on the effects of semitransparent walls on the natural convection flow field and temperature distribution in a rectangular enclosure. The physical model is shown in Fig. 1. The enclosure is formed by two horizontal adiabatic walls, and left and partition walls are semitransparent walls. The right wall is considered to be a blackbody diffuse surface. We assume the wall thicknesses, other than that of the semitransparent walls, to be negligible. The ambient temperature is set as 273 K and the external radiation temperature is assumed to be equal to T_a . The heat transfer coefficient between the ambient and left semitransparent walls is $10 \text{ W}/(\text{m}^2 \text{ K})$. The air inside the cavity is considered to be an incompressible Newtonian fluid that does not participate in the radiation process. The thickness of both semitransparent walls is 5 mm and their emissivity is 0.8. The height H of the enclosure is 500 mm and its length L is 300 mm. The aspect ratio of the cavity is computed as the length over its height, which in this case is $L/H=0.6$. In order to have a comprehensive understanding, two different physical models have been studied. In Case 1, the blackbody diffuse wall is considered as an isothermal wall and its temperature is 313 K, as shown in Fig. 1a. In Case 2, the direction of the radiation beam is perpendicular to the left boundary and I is prescribed as $1000 \text{ W}/\text{m}^2$, as shown in Fig. 1b.

Numerical Simulation

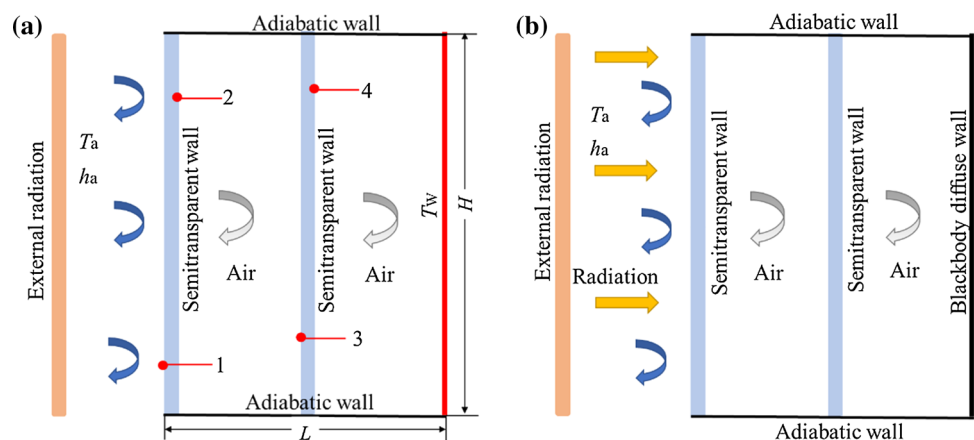
Math Theory

For two-dimensional steady flow and heat transfer of the presented physical model, the governing equations are listed as follows.

Continuity equation:

$$\frac{\partial u_i}{\partial x_i} = 0 \quad (1)$$

Fig. 1 Schematic of physical models. **a** Case 1, **b** case 2



Momentum equation:

$$\frac{\partial(u_i u_j)}{\partial x_j} = -\frac{1}{\rho} \frac{\partial p}{\partial x_i} + \frac{1}{\rho} \frac{\partial}{\partial x_j} \left[\mu \left(\frac{\partial u_i}{\partial x_j} + \frac{\partial u_j}{\partial x_i} \right) - \overline{\rho u'_i u'_j} \right] - g\beta(T - T_0) \tag{2}$$

Energy equation:

$$\frac{\partial(u_j T)}{\partial x_j} = \frac{1}{\rho} \frac{\partial}{\partial x_j} \left(\frac{\lambda}{c_p} \frac{\partial T}{\partial x_j} - \overline{\rho u'_j T'} \right) \tag{3}$$

where p is the pressure; T' is the fluctuating temperature; u_i and u_j are the mean velocity components in the i and j directions, respectively; u'_i and u'_j are the corresponding fluctuating velocity components in the i and j directions, respectively; $(-\overline{\rho u'_i u'_j})$ is the Reynolds stress; and $(\overline{u'_j T'})$ is the turbulence heat flux.

The choice of turbulence model is dictated not only by the type of flow but also by the availability of computational power and the desired accuracy. Buoyancy-driven air flow in the regular enclosure is the index for selecting a turbulence model. RANS models have been widely used in turbulent fluid flow simulations, and they demand a reasonable level of computational resources. In this paper, the two-equation renormalization group (RNG) $k-\epsilon$ model is selected to predict the turbulence in the cavity, as previous studies have reported this model to be computationally efficient and stable [29]. The turbulence kinetic energy, k , and the dissipation rate, ϵ , are obtained from the following transport equations:

$$\frac{\partial}{\partial x_i} (\rho k u_i) = \frac{\partial}{\partial x_j} \left(\alpha_k \mu_{\text{eff}} \frac{\partial k}{\partial x_j} \right) + G_k + G_b - \rho \epsilon - Y_M \tag{4}$$

$$\frac{\partial}{\partial x_i} (\rho \epsilon u_i) = \frac{\partial}{\partial x_j} \left(\alpha_\epsilon \mu_{\text{eff}} \frac{\partial \epsilon}{\partial x_j} \right) + C_{1\epsilon} \frac{\epsilon}{k} (G_k + C_{3\epsilon} G_b) - C_{2\epsilon} \rho \frac{\epsilon^2}{k} - R_\epsilon \tag{5}$$

where G_k represents the production of turbulence kinetic energy; G_b represents the generation of ϵ ; Y_M represents the contribution of fluctuating dilatation in the compressible turbulence to the overall dissipation rate; and α_k and α_ϵ are the inverse effective Prandtl numbers for k and ϵ , respectively.

$$G_b = \beta g \frac{\mu_t}{\sigma_t} \frac{\partial T}{\partial x_i} \tag{6}$$

$$G_k = \mu_t \left(\frac{\partial u_i}{\partial x_j} + \frac{\partial u_j}{\partial x_i} \right) \frac{\partial u_i}{\partial x_j} - \frac{2}{3} \rho k \delta_{ij} \frac{\partial u_j}{\partial x_i} \tag{7}$$

The turbulent viscosity μ_t can be obtained as:

$$\mu_t = C_\mu \frac{\rho k^2}{\epsilon} \tag{8}$$

R_ϵ is defined as:

$$R_\epsilon = \frac{C_\mu \rho \eta^3 (1 - \eta/\eta_0) \epsilon^2}{1 + \beta \eta^3} \frac{\epsilon^2}{k} \tag{9}$$

where $\eta = Sk/\epsilon$, $S = \sqrt{2S_{ij}S_{ij}}$; $\eta_0 = 4.38$, $\beta = 0.012$, $C_{1\epsilon} = 1.42$, $C_{2\epsilon} = 1.68$, $C_{3\epsilon} = 1$ and $C_\mu = 0.0845$ [30].

In this study, the radiation problem is solved through using the DO radiation model. More importantly, only the DO model allows to solve semitransparent walls [31]. We used the DO model to solve the radiation transport equation (RTE) (given below) for a finite number of discrete solid angles, each associated with a vector direction s fixed in the global Cartesian system (x, y, z) . The RTE in the direction s is written as follows:

$$\nabla \cdot (I(\mathbf{r}, s) \mathbf{s}) + (a + \sigma_s) I(\mathbf{r}, s) = an^2 \frac{\sigma T^4}{\pi} + \frac{\sigma_s}{4\pi} \int_0^{4\pi} I(\mathbf{r}, s') \Phi(s \cdot s') d\Omega' \tag{10}$$

where \mathbf{r} represents the position vector; s' represents the scattering direction vector.

The conduction heat transfer equation of a semitransparent wall is given by the following equation:

$$\frac{\partial}{\partial x} \left(\frac{k_{\text{semi}}}{\rho_{\text{semi}} c_{p_{\text{semi}}}} \frac{\partial T_{\text{semi}}}{\partial x} \right) + \frac{\partial}{\partial y} \left(\frac{k_{\text{semi}}}{\rho_{\text{semi}} c_{p_{\text{semi}}}} \frac{\partial T_{\text{semi}}}{\partial y} \right) + S^T = 0 \tag{11}$$

Once the intensity radiation field is known, the source term S^T in the conduction heat transfer equation can be calculated as follows:

$$S^T = \int_{\Omega_i=4\pi} I(S, S_i) \Omega d\Omega_i \tag{12}$$

Grid Test

To numerically model turbulent natural convection, it is best to use many nodes near the boundaries of solid walls [32]. Therefore, we used a boundary layer with an initial size of 0.06 mm and a growth factor of 1.2 to capture the fluid flow that develops near the wall, as shown in Fig. 2. Grid independence in the solution scheme significantly affects the calculation results of the heat transfer and fluid flow. In order to verify the validity of the grid sensitivity, different mesh sizes are used to test grid independence. The heat flux (case 1) of wall-1 and average temperature of T_w (case 2) for different mesh sizes are monitored and the results are shown in Table 1. It is found that almost the same temperature and heat flux for the two cases are obtained for different mesh sizes. Based on this result, we selected the mid-range mesh size of 180×160 for the simulation analysis.

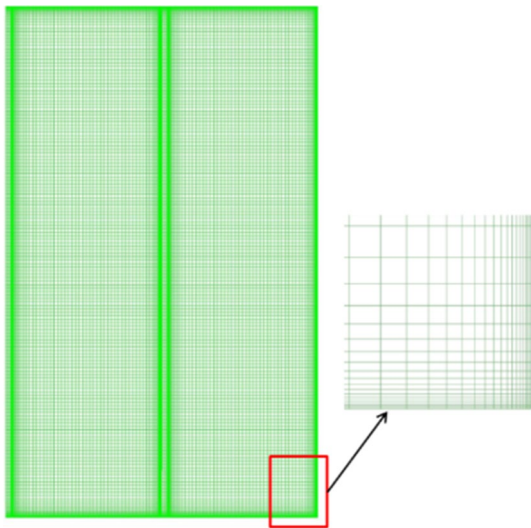


Fig. 2 Grid

Table 1 Grid test

Grid size	q_1 (W/m ²) (Case 1)	T_w (K) (Case 2)
150 × 130	212.461	360.799
180 × 160	212.408	360.788
240 × 220	212.374	360.785

Boundary Conditions

To solve governing equations, appropriate boundary conditions are necessary. The model is subjected to different types of boundary conditions and all walls are considered as non-slip wall boundary. The detailed boundary conditions can be obtained as follows:

$$\text{Wall 1 : } h_a(T_1 - T_a) + \sigma \epsilon_{\text{semi}}(T_1^4 - T_a^4) = -\lambda_{\text{semi}} \frac{\partial T_{\text{semi-left}}}{\partial x} \tag{13}$$

$$\text{Wall 2 : } -\lambda_{\text{semi}} \frac{\partial T_{\text{semi-left}}}{\partial x} = -\lambda \frac{\partial T}{\partial x} + q_{2,\text{rad}} + q_{2,\text{conv}} \tag{14}$$

$$\text{Wall 3 : } -\lambda \frac{\partial T}{\partial x} + q_{3,\text{rad}} + q_{3,\text{conv}} = -\lambda_{\text{semi}} \frac{\partial T_{\text{semi-mid}}}{\partial x} \tag{15}$$

$$\text{Wall 4 : } -\lambda_{\text{semi}} \frac{\partial T_{\text{semi-mid}}}{\partial x} = -\lambda \frac{\partial T}{\partial x} + q_{4,\text{rad}} + q_{4,\text{conv}} \tag{16}$$

$$\text{Wall 5 : } T_1 = T_w \text{ (Case 1)} \tag{17}$$

$$\tau^2 q_{\text{in}} + q_{w,\text{rad}} + q_{w,\text{conv}} = 0 \text{ (Case 2)} \tag{18}$$

$$\text{Top and bottom walls : } q_{\text{rad}} + q_{\text{conv}} = 0 \tag{19}$$

where $q_{2,\text{rad}}$, $q_{3,\text{rad}}$, $q_{4,\text{rad}}$, and $q_{w,\text{rad}}$ are the radiative heat flux of wall-2, wall-3, wall-4, and the blackbody diffuse wall, respectively, W/m²; $q_{2,\text{conv}}$, $q_{3,\text{conv}}$, $q_{4,\text{conv}}$ and $q_{w,\text{conv}}$ are the convective heat flux of wall-2, wall-3, wall-4, and the blackbody diffuse wall, respectively, W/m².

In this study, we investigated the impact of a single factor on the enclosure. Thus, only the study object changes in the simulation and other factors are held constant. These constant values for the simulated parameters included the transmittance and thermal conductivity of the semitransparent wall, whose values were 0.8 and 0.5 W/(m·K), respectively.

Modeling Strategy

We performed all calculations reported hereafter using the general-purpose commercial code FLUENT, based on the finite-volume method. The governing equations were discretized by the finite-volume method on a non-uniform staggered grid system using the SIMPLEC algorithm. PRESTO! scheme was used for the pressure discretization. The second-order upwind scheme was considered for the momentum and energy equations.

Results and Discussion

Model Verification

To evaluate the validity of the numerical model, we conducted a simulation according to the work in Ref. [5]. A comparison of the temperature distribution at mid-height of enclosure is given in Fig. 3. The *R-square* method is used to compare the simulation results with the experimental measurements, and the equation is Eq. (20). The value of

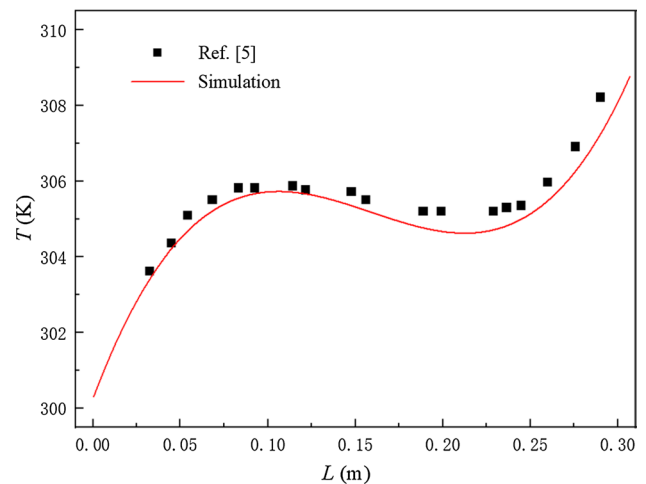


Fig. 3 Comparison of temperature distribution at mid-height of enclosure with the experimental results in Ref. [5]

R-square is 0.8783, which means that there is good agreement between the reference's results and the computational fluid dynamics (CFD) predicted data.

$$R\text{-square} = 1 - \frac{\sum_{i=1}^n (y_{\text{sim},i} - y_{\text{exp},i})^2}{\sum_{i=1}^n (y_{\text{exp},i} - \bar{y}_{\text{exp},i})^2} \quad (20)$$

where $y_{\text{sim},i}$ is the simulation data, $y_{\text{exp},i}$ is the experimental data from Ref. [5], and $\bar{y}_{\text{exp},i}$ is the mean value of the experimental data.

Effect of Single and Double Semitransparent Walls

Case 1

The temperature fields of the enclosure with and without a semitransparent partition are shown in Fig. 4. For the non-partition enclosure, the temperature is distributed evenly from bottom to top and the isotherms are substantially parallel, except for the highest one. For the partitioned enclosure, it is observed that the temperature field is divided into two parts, with the temperature of the right part (E_2) much higher than that of the left part (E_1). The average temperature of the left semitransparent wall (S_{left}) decreased by about 3.02 K, as compared to that of the enclosure without a partition. The heat flux on wall-1 is 22.4% lower in the partitioned enclosure, which means that the heat transfer in a partitioned rectangular cavity is considerably lower than that in a non-partitioned cavity. This numerical result indicates that a semitransparent partition can decrease heat loss effectively. The flow patterns of the enclosure with and without a

semitransparent partition are shown in Fig. 5. At the center of the cavity, the streamlines are nearly horizontal, which indicates fluid stratification, but at the boundaries adjacent to the adiabatic walls there are significant differences, as shown in Fig. 5a. In contrast, in Fig. 5b, the streamlines are not parallel. The maximum stream function value of E_2 is greater than that of E_1 .

Case 2

The temperature distributions of an enclosure with and without a semitransparent partition under a constant radiation flux are shown in Fig. 6. A uniform temperature gradient is observed in Fig. 6a. The temperature field of the enclosure with double semitransparent walls can be considered to have two parts, and the average temperature of E_2 is 21.9 K higher than that of E_1 . This result indicates that T_w of the enclosure with double semitransparent walls is 360.8 K, as compared to 359.7 K for that with a single wall. This means that an additional semitransparent partition is beneficial for improving the absorbed temperature. Figure 7 shows the stream functions for single and double semitransparent walls, respectively. In Fig. 7a, the flow pattern is very similar to that in Fig. 5a. For double semitransparent walls, the stream function of E_1 is higher than that of E_2 , and the streamlines tend to more turbulence than that occurring with a single wall.

The comparison of T_w at different transmittances (τ) in an enclosure with and without a semitransparent partition wall is shown in Fig. 8. There appears to be a positive correlation between τ and T_w for both research objects. When τ drops to 0.5, the T_w value of the enclosure without a semitransparent

Fig. 4 Temperature contours for case 1. **a** Single semitransparent wall, **b** double semitransparent walls

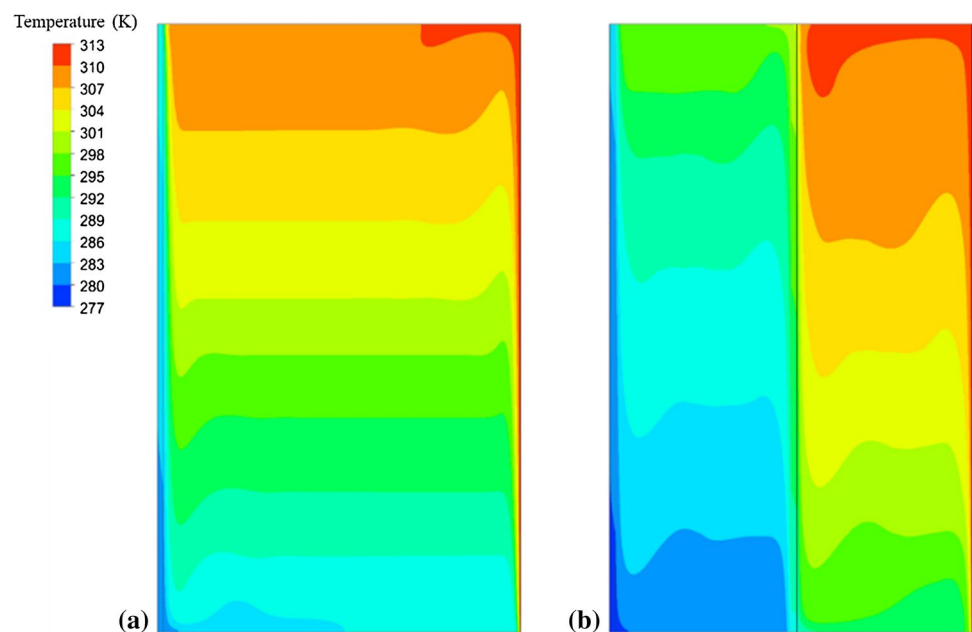


Fig. 5 Stream functions for case 1. **a** Single semitransparent wall, **b** double semitransparent wall

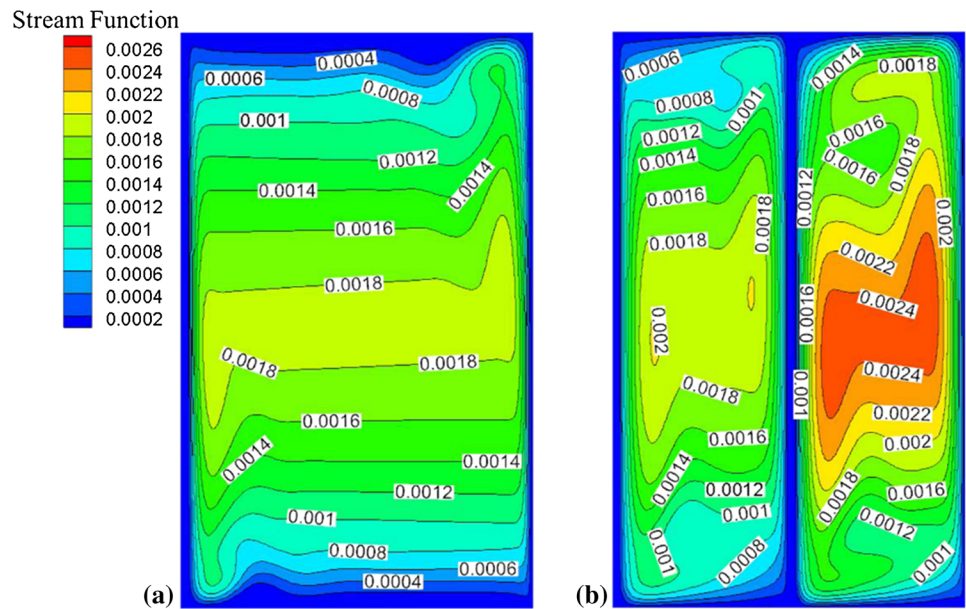
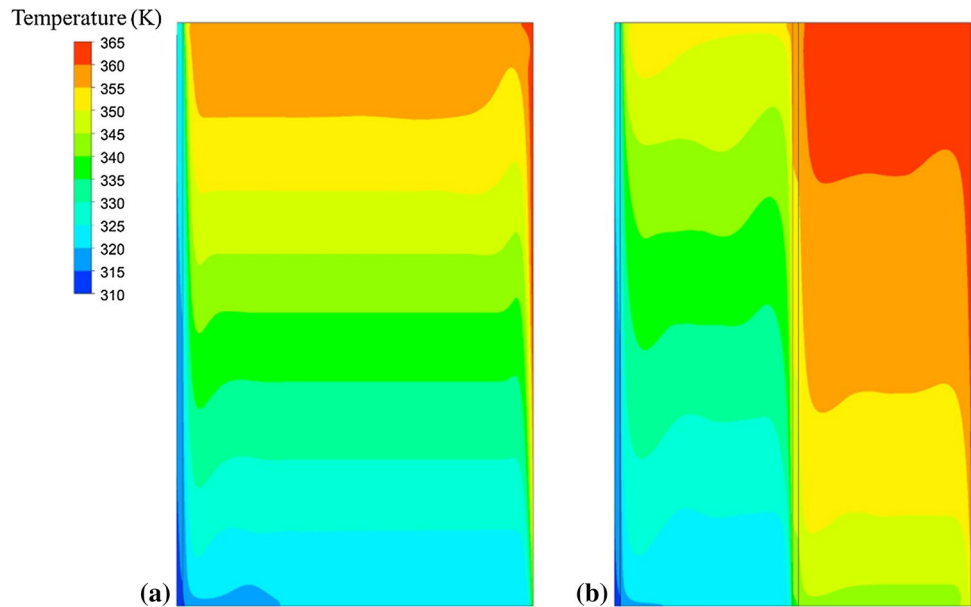


Fig. 6 Temperature contours for case 2. **a** Single semitransparent wall, **b** double semitransparent walls



partition is slightly greater than that with such a wall. This indicates that with a decrease in the transmittance, a semitransparent partition would fail to maintain a higher temperature distribution.

Effect of Semitransparent and Opaque Partitions

Figure 9 displays the temperature fields of enclosures with semitransparent and opaque partition walls, respectively, in which it is obvious that the temperature of an enclosure with a semitransparent partition is higher than that with an opaque partition. The average temperature of

E_1 for a semitransparent partition is 4.2 K higher than that for an opaque partition. This is because radiation can be transmitted by the semitransparent partition from wall-4 to wall-3. However, with an opaque partition, the heat transfer process to wall-3 can only occur by conduction. The simulation results show that the heat fluxes from the left semitransparent wall are 212.4 W/m^2 and 142.1 W/m^2 for semitransparent and opaque partitions, respectively. As shown in Fig. 10, the stream function value in E_1 with a semitransparent partition is higher than that in one with an opaque wall, and lower than that in the right part.

Fig. 7 Stream functions for case 2. **a** Single semitransparent wall, **b** double semitransparent walls

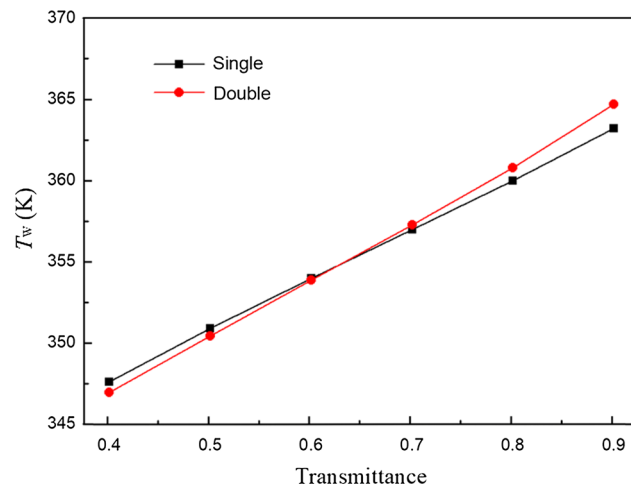
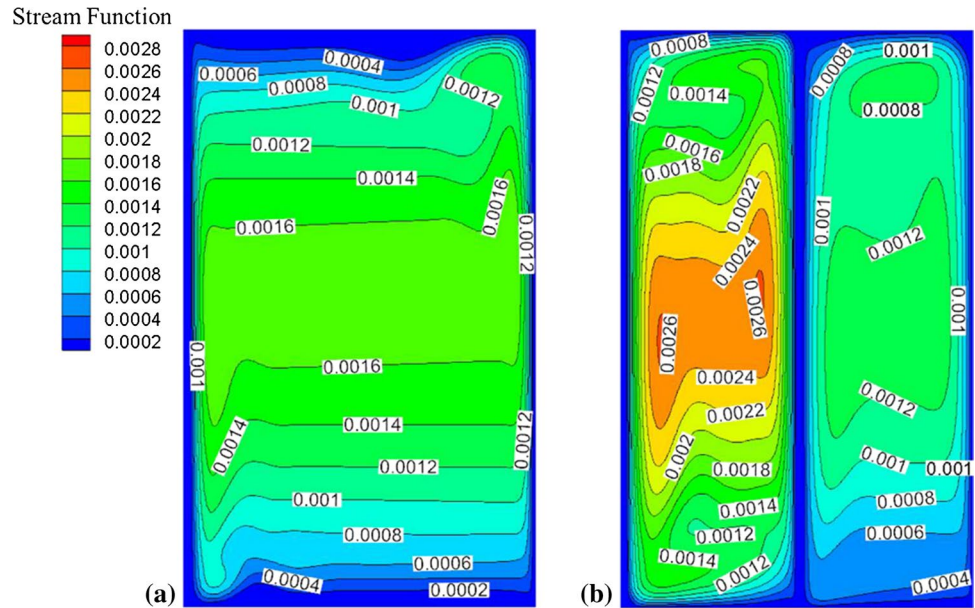


Fig. 8 Comparison of T_w values at different transmittances

Effect of Transmittance

The transmittance of a semitransparent wall has a significant effect on the thermal and flow characteristics in an enclosure. In this section, different combinations of transmittance in an enclosure with two semitransparent walls have been studied. The transmittance combination is expressed as $(\tau_{left}, \tau_{mid})$.

Case 1

Figure 11 shows the temperature contours of four transmittance combinations, in which we can see that the isotherms in E_1 are similar in all cases. In addition, when the transmittance of S_{mid} is varied from 0.6 to 0.9, the higher temperature

region in E_2 is expanded, and the lower temperature region is constricted. The comparison among the temperatures of E_1 , E_2 , S_{left} and S_{mid} is shown in Fig. 12, in which we can also observe that the temperatures of E_1 and S_{left} increase with the greater transmittance of the semitransparent partition. This is because the ability of the semitransparent material to transfer and distribute radiative energy intensifies the temperature distribution in the enclosure which becomes more homogeneous [5]. The results also show that the heat flux from wall-1 of (0.6, 0.6) is 34.5 W/m^2 greater than that of (0.9, 0.9). For the combinations of (0.6, 0.9) and (0.9, 0.6), the heat fluxes are almost the same. In Fig. 13, the stream function is shown for the four cases in which we find that the flow patterns are basically similar.

Case 2

Figure 14 shows the temperature contours of four transmittance combinations under a constant radiation flux. The comparison among the temperatures of E_1 , E_2 , S_{left} , and S_{mid} is shown in Fig. 15. For a normal constant radiation flux on wall-1, the high-temperature region in E_2 expands with an increase in the transmittance. The temperature gradient is reduced in E_1 as τ_{left} decreases from 0.9 to 0.6. For the combinations (0.6, 0.9) and (0.9, 0.6), it could be found that the temperature of E_2 for (0.9, 0.6) is much higher than that for (0.6, 0.9), as shown in Fig. 14b, c. However, the T_w of (0.9, 0.6) is 1.5 K lower than that of (0.9, 0.9), with the average temperature of E_2 for (0.9, 0.6) being 0.7 K greater than the latter. Figure 16 shows the stream functions for the four cases, in which we can see that the flow pattern in E_1 is similar to all four cases. The stream function values in E_2 are less than half of those in E_1 , which means the flow is weak.

Fig. 9 Temperature contours. **a** Semitransparent wall, **b** opaque wall

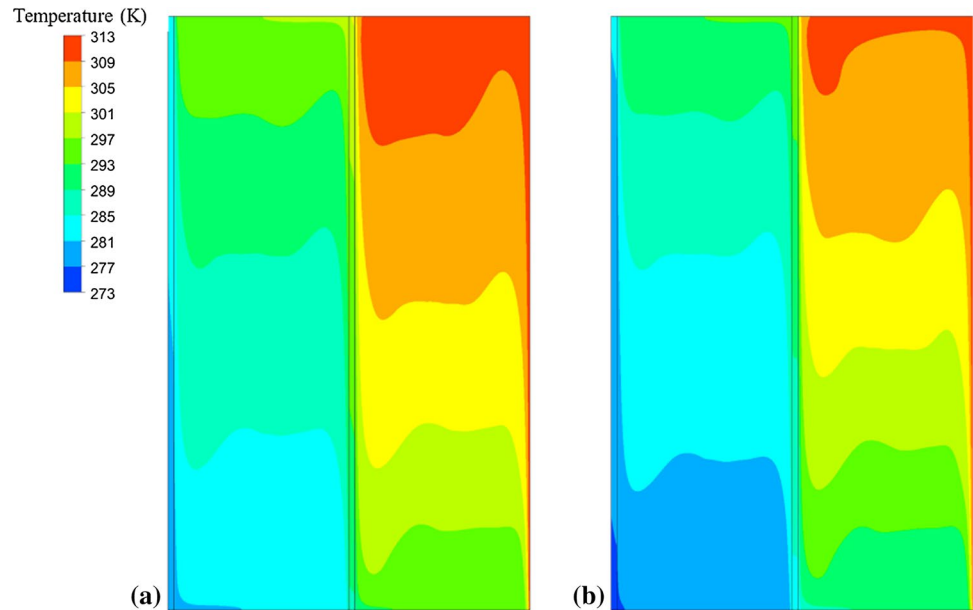
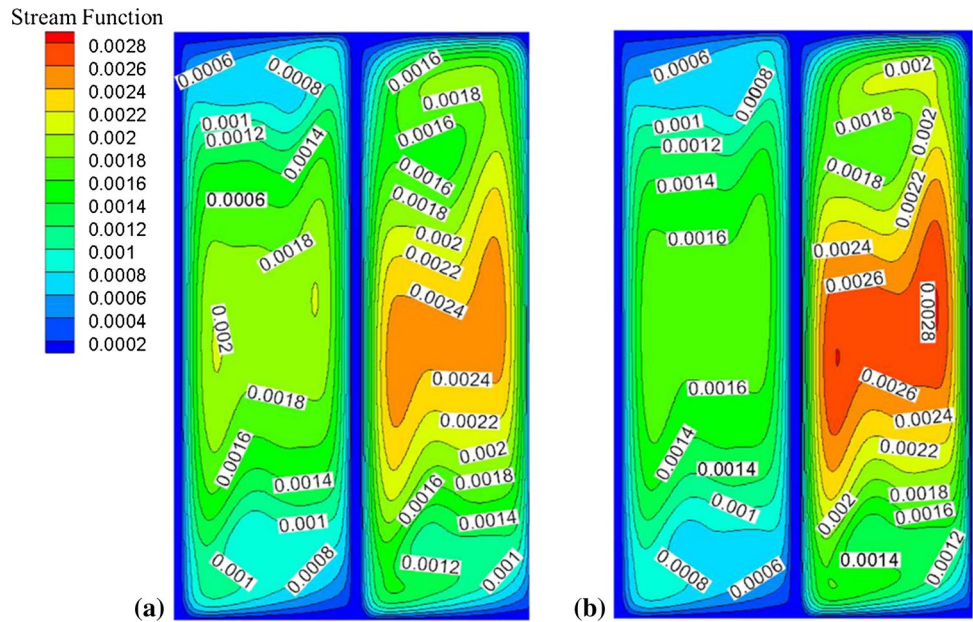


Fig. 10 Stream functions. **a** Semitransparent wall, **b** opaque wall



Effect of Thermal Conductivity

Case 1

The temperature profiles of different walls are shown in Fig. 17a and b, in which we can see that T_1 and T_3 increase quickly when λ increases from 0.05 to 0.5 W/(m·K). However, as λ continues to increase, the rate of increase in T_1 and T_3 slows and then becomes stable. In contrast, T_2 and T_4 decrease rapidly as λ increases from 0.05 to 0.5 W/(m·K), then begins to stabilize. Figure 17c shows the variation in the heat flux in wall-1 with the thermal conductivity of the semitransparent wall. In the figure, we can see that

the heat flux increases rapidly when λ ranges from 0.05 to 0.5 W/(m·K), then tends to remain constant as λ continues to increase. The vertical velocity distributions at $H/2$ for different thermal conductivities are shown in Fig. 17d. If we compare the vertical velocities in E_1 , the lowest vertical velocity occurs at 0.05 W/(m·K) and the others are almost the same. The vertical velocity in E_2 is the highest.

Case 2

As shown in Fig. 18a and b, T_1 increases quickly when λ increases from 0.05 to 0.5 W/(m·K). However, as λ continues to increase, the change in T_1 slows and tends to

Fig. 11 Temperature contours of four transmittance combinations for case 1. **a** (0.6, 0.6), **b** (0.6, 0.9), **c** (0.9, 0.6), and **d** (0.9, 0.9)

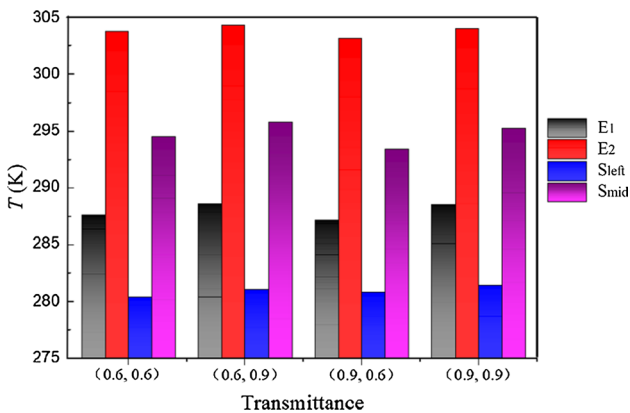
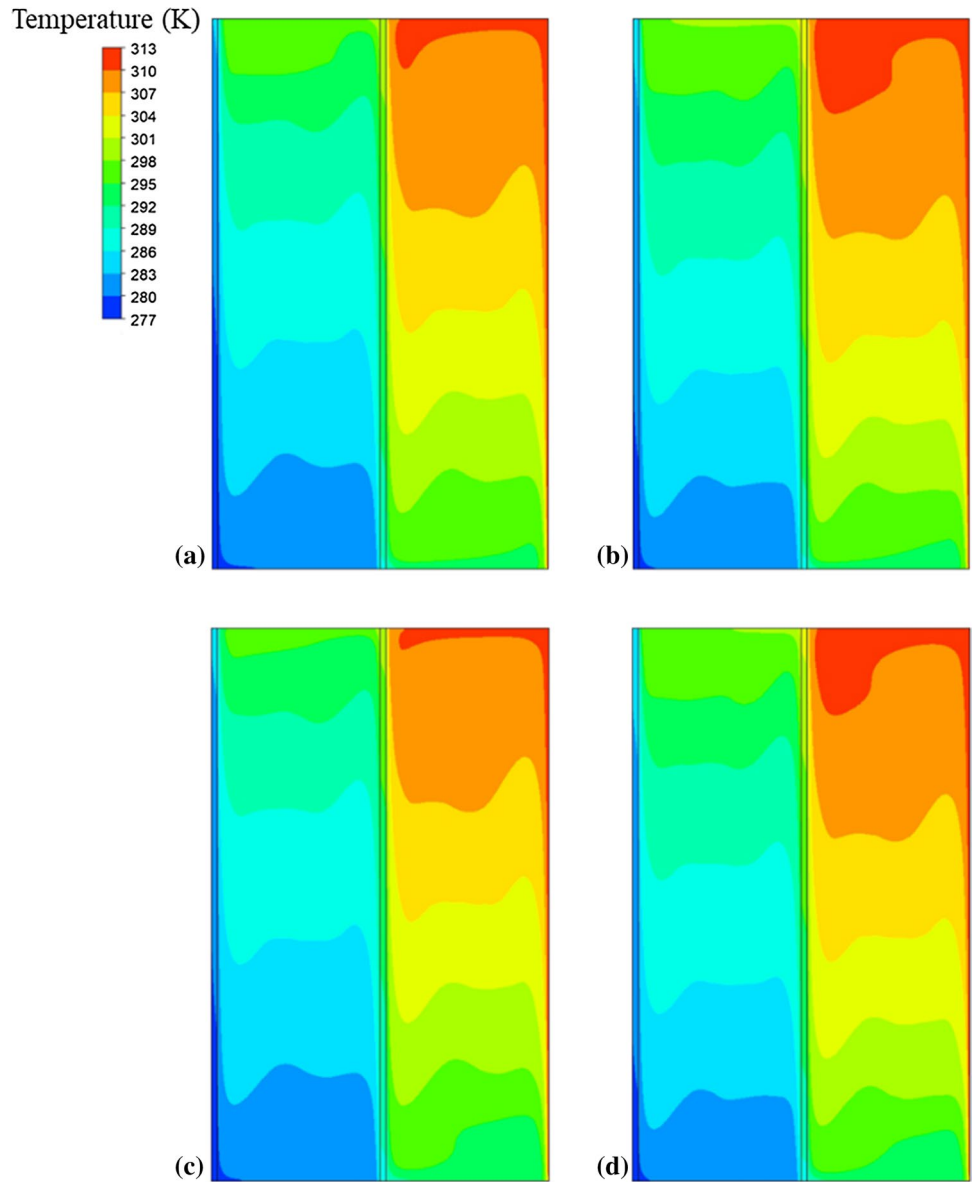
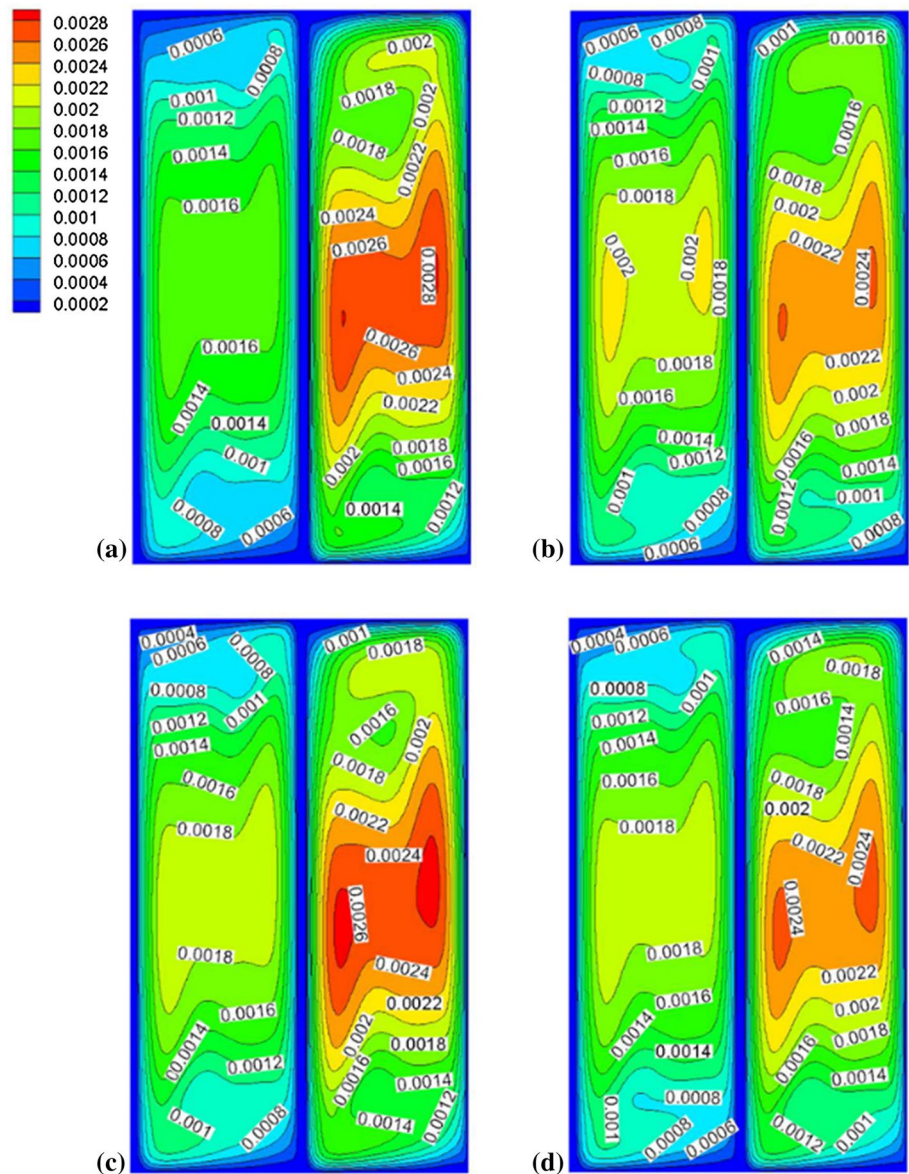


Fig. 12 Temperature comparison of E_1 , E_2 , S_{left} , and S_{mid} for case 1

become stable. In contrast, T_2 , T_3 , and T_4 decrease rapidly as λ increases from 0.05 to 0.5 W/(m·K), and then begin to stabilize. In Fig. 18c, when λ increases from 0.05 to 0.5 W/(m·K), T_w decreases quickly. As λ continues to increase, the change in T_1 slows and tends to become stable. T_2 , T_3 , T_4 , and T_w demonstrate the same pattern, which indicates that a higher temperature distribution would be achieved when λ decreases below a critical value. When the thermal conductivity of a semitransparent wall is greater than 0.5 W/(m·K), the change is weak. Figure 18d shows the vertical velocity distributions at $H/2$ for different thermal conductivities, in which we can see that the velocity is low for $\lambda = 0.05$ W/(m·K) in the two parts, and little difference is observed in the others.

Fig. 13 Stream functions for case 1. **a** (0.6, 0.6), **b** (0.6, 0.9), **c** (0.9, 0.6), and **d** (0.9, 0.9)

Stream Function



Conclusion

In this paper, we presented our study of the natural convection flow field and temperature distribution in a rectangular enclosure with semitransparent walls. Two different cases were considered based on their boundary conditions, the first was the isothermal for an opaque wall, and the other was the radiation flux on the left semitransparent wall. RNG $k-\epsilon$ model was adopted to simulate the turbulent flow in the enclosure. To compute the radiation heat transfer in a semitransparent medium, the discrete ordinates model was used. Then, we compared enclosures with single and double semitransparent walls and analyzed the different results obtained using semitransparent and opaque partitions. In addition, the effects of the transmittance and thermal conductivity

of a semitransparent wall on the fluid flow and temperature distribution in an enclosure have been investigated. From our simulation results, we can draw the following major conclusions.

- (1) The presence of a semitransparent partition has a significant impact on the flow field and temperature distribution, as compared to an enclosure without any partition. This result indicates that a semitransparent partition is beneficial for reducing heat loss, as shown in Case 1, and for obtaining a higher temperature distribution, as shown in Case 2.
- (2) From our comparison of an enclosure with either semitransparent or opaque walls, the results indicate that semitransparency allows radiation to pass through the

Fig. 14 Temperature contours for case 2. **a** (0.6, 0.6), **b** (0.6, 0.9), **c** (0.9, 0.6), and **d** (0.9, 0.9)

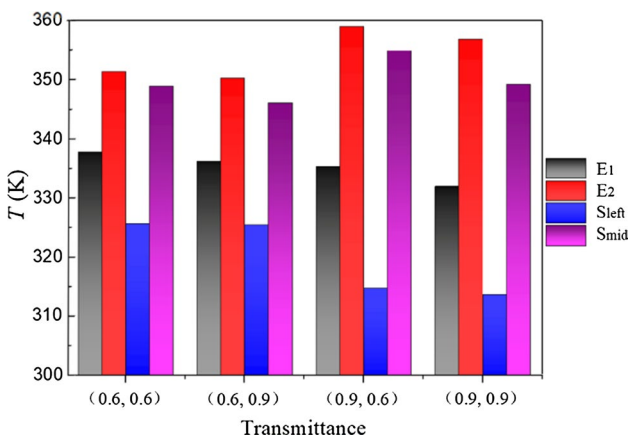
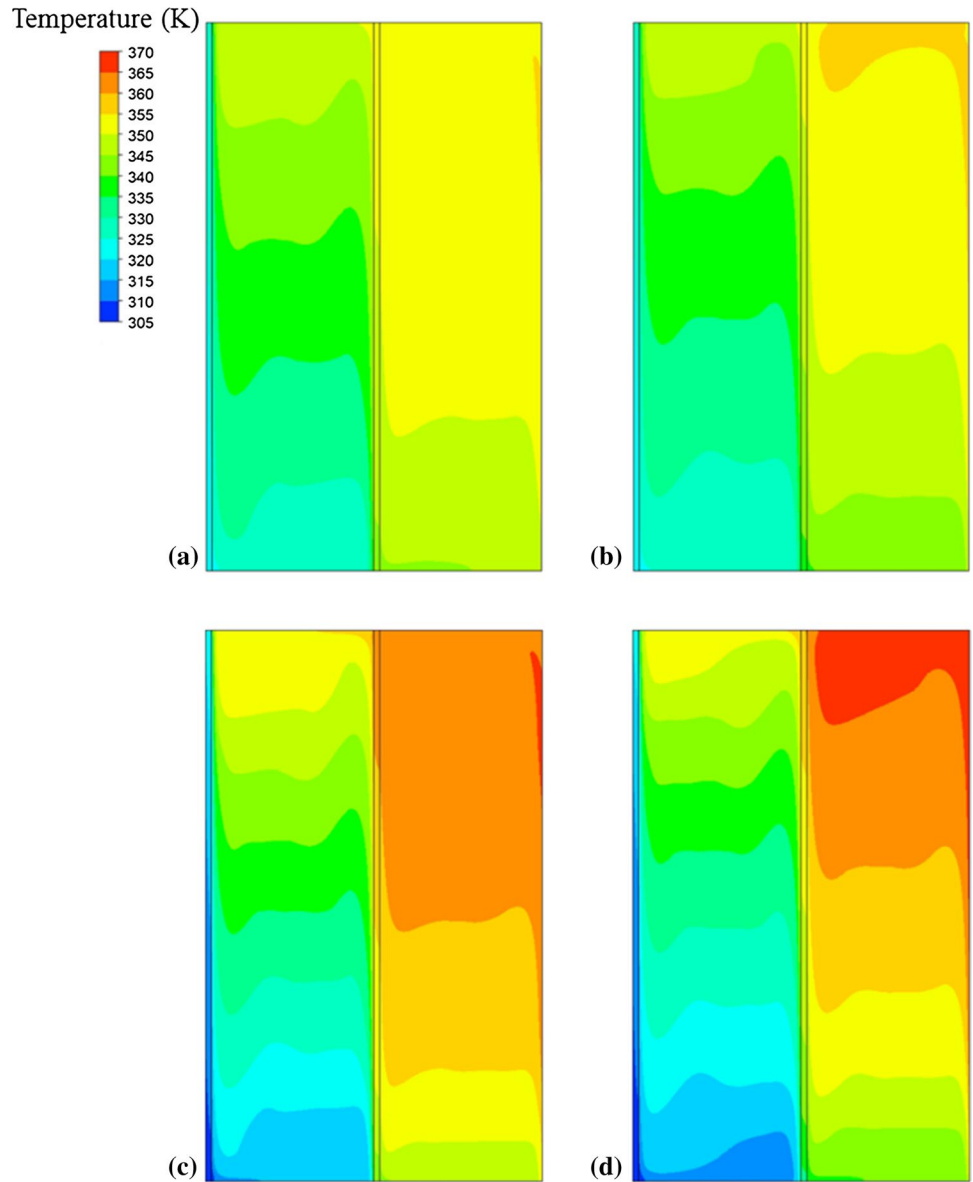
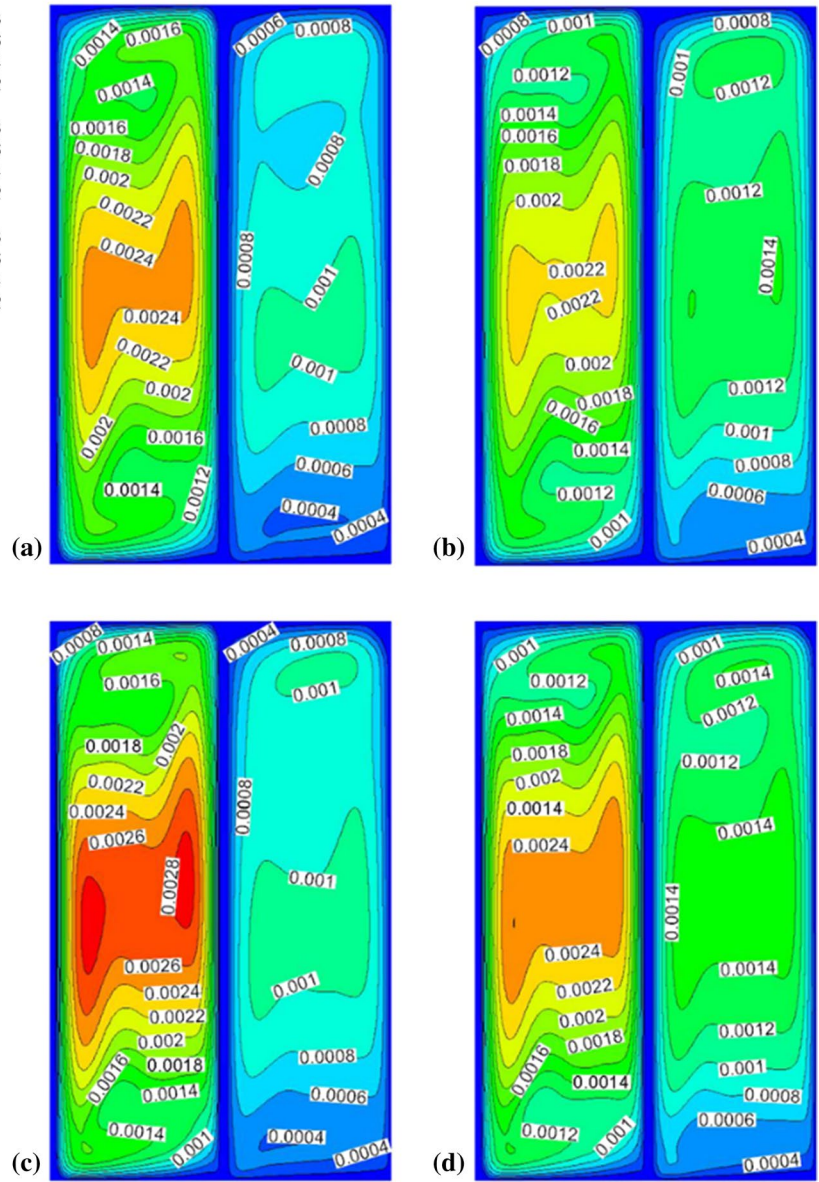
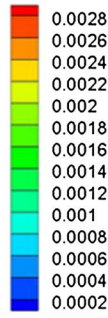


Fig. 15 Comparison of temperature of E_1 , E_2 , S_{left} , and S_{mid} for case 2

- (3) The transmittance of a semitransparent wall has a great effect on the thermal and flow characteristics in an enclosure.
- (4) The change in wall temperature is significant, with thermal conductivity values ranging from 0.05 to 0.5 W/(m·K), and is slight with values ranging from 0.5 to 10 W/(m·K) for both cases. For Case 1, the heat flux also increases rapidly for λ values ranging from 0.05 to 0.5 W/(m·K) and tends to become constant as λ continues to increase.

Fig. 16 Stream functions for case 2. **a** (0.6, 0.6), **b** (0.6, 0.9), **c** (0.9, 0.6), and **d** (0.9, 0.9)

Stream Function



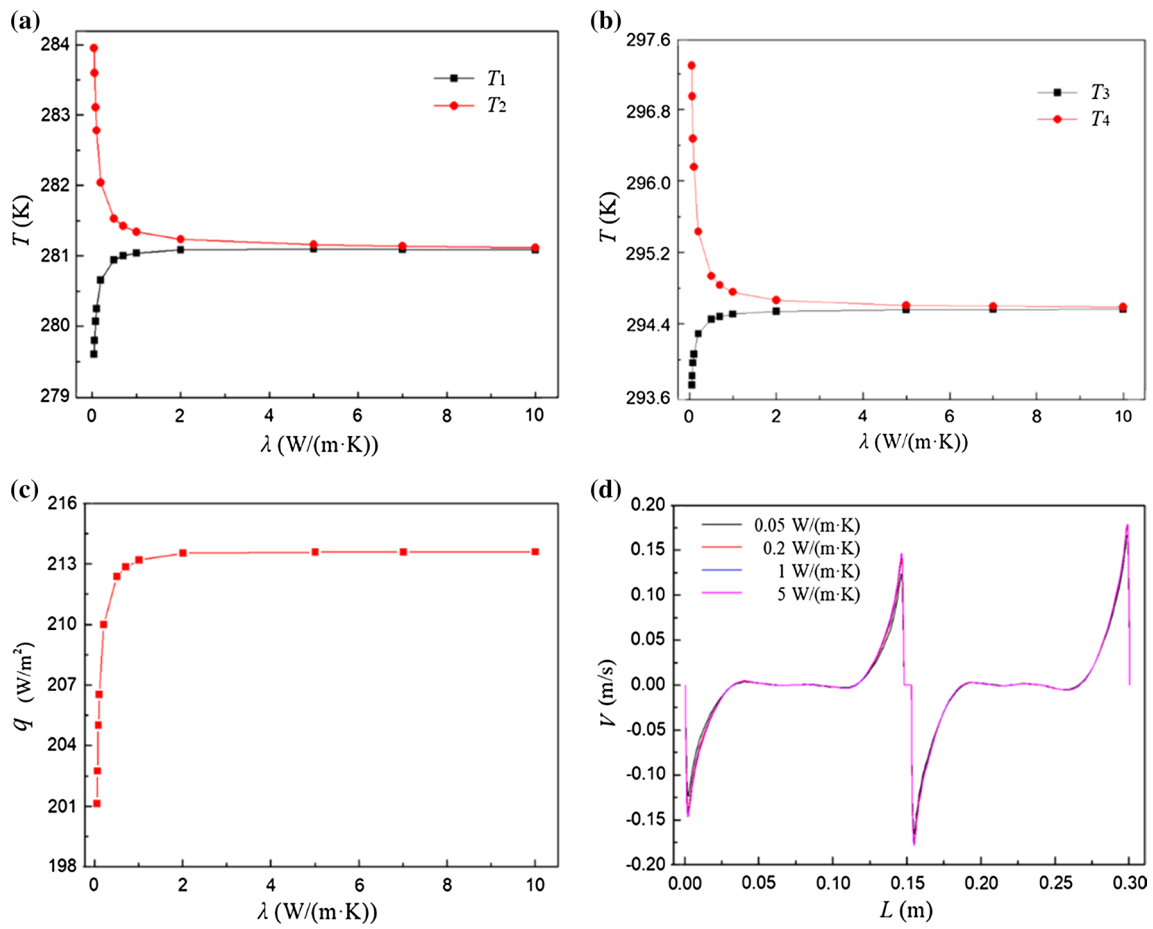


Fig. 17 Comparison of the variation profiles with various thermal conductivities for case 1. **a** T_1 and T_2 , **b** T_3 and T_4 , **c** heat flux from left semi-transparent wall, and **d** vertical velocity at $H/2$

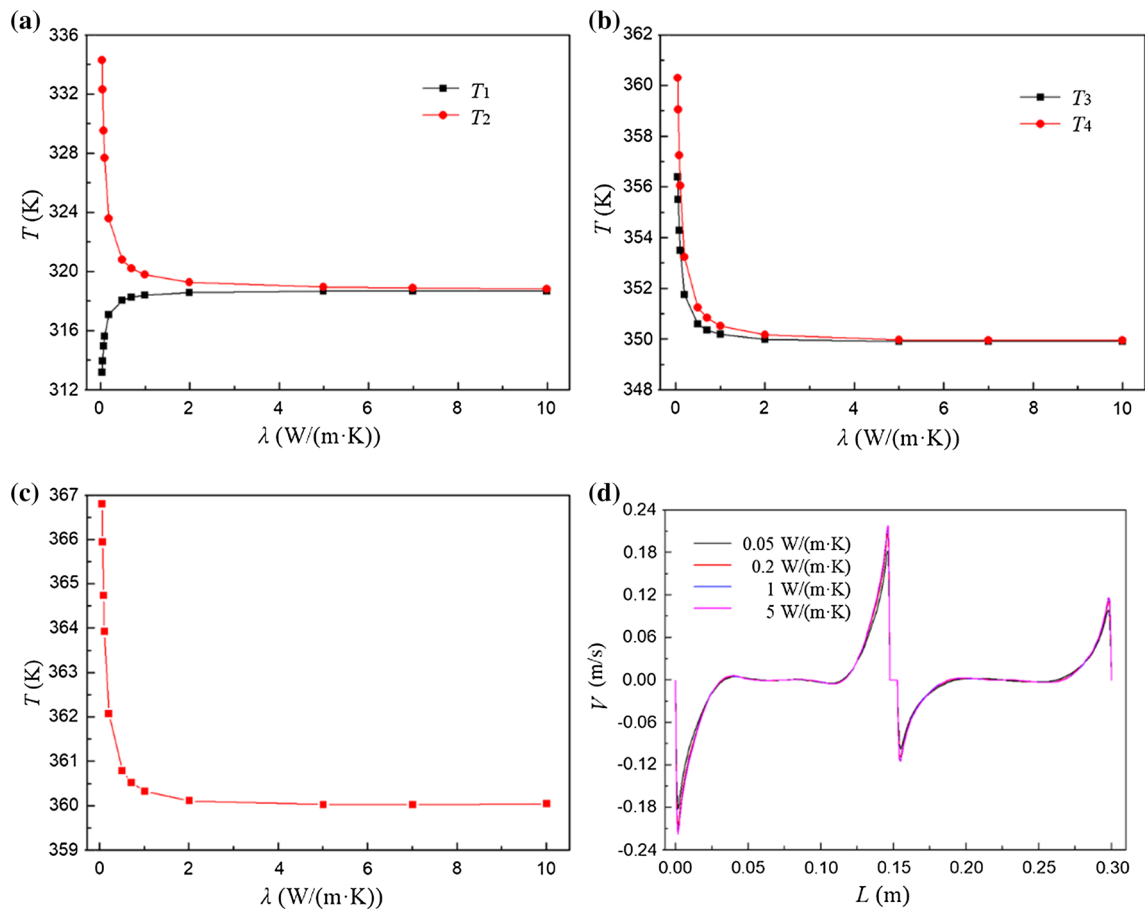


Fig. 18 Comparison of the variation profiles with various thermal conductivities for Case 2. **a** T_1 and T_2 , **b** T_3 and T_4 , **c** T_w , **d** vertical velocity at $H/2$

Acknowledgements This work was supported by the Shanghai Economic and Information Technology Committee Special Fund (CXY-2016-012). The simulation work was completed in cooperation with the High Performance Computing Center of Tianjin University, China.

Open Access This article is distributed under the terms of the Creative Commons Attribution 4.0 International License (<http://creativecommons.org/licenses/by/4.0/>), which permits unrestricted use, distribution, and reproduction in any medium, provided you give appropriate credit to the original author(s) and the source, provide a link to the Creative Commons license, and indicate if changes were made.

References

- Miroshnichenko IV, Sheremet MA (2018) Turbulent natural convection heat transfer in rectangular enclosures using experimental and numerical approaches: a review. *Renew Sustain Energy Rev* 82:40–59
- Ghosh A, Norton B (2018) Advances in switchable and highly insulating autonomous (self-powered) glazing systems for adaptive low energy buildings. *Renew Energy* 126:1003–1031
- Moreno B, Hernández JA (2018) Analytical solutions to evaluate solar radiation overheating in simplified glazed rooms. *Build Environ* 140:162–172
- Flores JJ, Alvarez G, Xaman JP (2008) Thermal performance of a cubic cavity with a solar control coating deposited to a vertical semitransparent wall. *Sol Energy* 82:588–601
- Li D, Ai Q, Xia X et al (2013) Optical constants effect on laminar natural convection and radiation in rectangular enclosure with one vertical semitransparent wall. *Int J Heat Mass Transf* 67:724–733
- Wu T, Lei C (2016) Thermal modelling and experimental validation of a semi-transparent water wall system for Sydney climate. *Sol Energy* 136:533–546
- Xamán J, Arce J, Álvarez G et al (2008) Laminar and turbulent natural convection combined with surface thermal radiation in a square cavity with a glass wall. *Int J Therm Sci* 47:1630–1638
- Xamán J, Álvarez G, Hinojosa J et al (2009) Conjugate turbulent heat transfer in a square cavity with a solar control coating deposited to a vertical semitransparent wall. *Int J Heat Fluid Flow* 30:237–248
- Noh-Pat F, Xamán J, Álvarez G et al (2015) Unsteady-RANS simulation of conjugate heat transfer in a cavity with a vertical semitransparent wall. *Comput Fluids* 117:183–195

10. González-Julián E, Xamán J, Moraga NO et al (2018) Annual thermal evaluation of a double pane window using glazing available in the Mexican market. *Appl Therm Eng* 143:100–111
11. Xamán J, Pérez-Nucamendi C, Arce J et al (2014) Thermal analysis for a double pane window with a solar control film for using in cold and warm climates. *Energy Build* 76:429–439
12. Xamán J, Olazo-Gómez Y, Zavala-Guillén I et al (2017) Thermal evaluation of a room coupled with a double glazing window with/without a solar control film for Mexico. *Appl Therm Eng* 110:805–820
13. Xamán J, Olazo-Gómez Y, Chávez Y et al (2016) Computational fluid dynamics for thermal evaluation of a room with a double glazing window with a solar control film. *Renew Energy* 94:237–250
14. Xamán J, Jiménez-Xamán C, Álvarez G et al (2016) Thermal performance of a double pane window with a solar control coating for warm climate of Mexico. *Appl Therm Eng* 106:257–265
15. Xamán J, Mejía G, Álvarez G et al (2010) Analysis on the heat transfer in a square cavity with a semitransparent wall: effect of the roof materials. *Int J Therm Sci* 49:1920–1932
16. Rabhi M, Bouali H, Mezrhab A (2008) Radiation–natural convection heat transfer in inclined rectangular enclosures with multiple partitions. *Energy Convers Manag* 49:1228–1236
17. Selimefendigil F, Öztop HF (2016) Conjugate natural convection in a cavity with a conductive partition and filled with different nanofluids on different sides of the partition. *J Mol Liq* 216:67–77
18. Sun Y, Lin G, Yu J et al (2018) Theoretical investigation of natural convection heat transfer in inclined and fully divided CO₂ enclosures on Mars. *Int J Heat Mass Transf* 126:1113–1122
19. Sambou V, Lartigue B, Monchoux F et al (2008) Theoretical and experimental study of heat transfer through a vertical partitioned enclosure: application to the optimization of the thermal resistance. *Appl Therm Eng* 28:488–498
20. Öztop HF, Zhao Z, Yu B (2009) Conduction-combined forced and natural convection in lid-driven enclosures divided by a vertical solid partition. *Int Commun Heat Mass Transf* 36:661–668
21. Khatamifar M, Lin W, Armfield SW et al (2017) Conjugate natural convection heat transfer in a partitioned differentially-heated square cavity. *Int Commun Heat Mass Transf* 81:92–103
22. Miroshnichenko IV, Sheremet MA, Mohamad AA (2016) Numerical simulation of a conjugate turbulent natural convection combined with surface thermal radiation in an enclosure with a heat source. *Int J Therm Sci* 109:172–181
23. Miroshnichenko IV, Sheremet MA, Chamkha AJ (2018) Turbulent natural convection combined with surface thermal radiation in a square cavity with local heater. *Int J Numer Methods Heat Fluid Flow* 28:1698–1715
24. Miroshnichenko IV, Sheremet MA (2018) Radiation effect on conjugate turbulent natural convection in a cavity with a discrete heater. *Appl Math Comput* 321:358–371
25. Miroshnichenko IV, Sheremet MA (2018) Turbulent natural convection combined with thermal surface radiation inside an inclined cavity having local heater. *Int J Therm Sci* 124:122–130
26. Wu T, Lei C (2015) On numerical modelling of conjugate turbulent natural convection and radiation in a differentially heated cavity. *Int J Heat Mass Transf* 91:454–466
27. Sharma AK, Velusamy K, Balaji C (2008) Interaction of turbulent natural convection and surface thermal radiation in inclined square enclosures. *Heat Mass Transf* 44:1153–1170
28. Mao YJ, Zhang YW (2013) Evaluation of turbulent models for natural convection of compressible air in a tall cavity. *Numer Heat Transf Part B Fundam* 64:351–364
29. Horikiri K, Yao Y, Yao J (2014) Modelling conjugate flow and heat transfer in a ventilated room for indoor thermal comfort assessment. *Build Environ* 77:135–147
30. Liu C, Lu Y, Zhou Y et al (2018) CFD simulation of the two-phase flow in a novel cooking tank for ethanol production. *Trans Tianjin Univ* 24:212–223
31. Colomer G, Costa M, Cònsul R et al (2004) Three-dimensional numerical simulation of convection and radiation in a differentially heated cavity using the discrete ordinates method. *Int J Heat Mass Transf* 47:257–269
32. Sun Y, Wen G, Xiao X et al (2018) Numerical study on heat transfer and flow characteristics for laminar flow in a circular tube with swirl generators. *Trans Tianjin Univ* 24:244–255